Energy 313 (2024) 133990

Contents lists available at ScienceDirect

Energy

journal homepage: www.elsevier.com/locate/energy

An explicit State-of-Charge planning solution for plug-in hybrid electric vehicle based on low-granularity prior-knowledge

Xuan Cai [a], Wei Zhou [b,*], Zhiyong Cui [a], Xuesong Bai [a], Fan Liu [c], Haiyang Yu [a], Yilong Ren [a]

[a] State Key Laboratory of Intelligent Transportation Systems, School of Transportation Science and Technology, Beihang University, Beijing, 100191, PR China
[b] School of Mechanical and Vehicular Engineering, Hunan University, Changsha, 410000, PR China
[c] School of Computing, National University of Singpore, Singpore, 119077, Singapore

ARTICLE INFO

Keywords:
State-of-Charge planning
Plug-in Hybrid Electric Vehicle
Predictive energy management
Pontryagin's Minimum Principle

ABSTRACT

The intervention of batteries in hybrid electric vehicles, when paired with an effective Energy Management Strategy (EMS), substantially improves fuel efficiency and reduces emissions in comparison to conventional internal combustion engine vehicles. The evolution of Intelligent Transportation Systems (ITS) has facilitated the possibility of predictive energy management (PEM) predicated on State-of-Charge (SoC) planning. Nevertheless, prevalent methodologies frequently encounter challenges in balancing optimization with real-time applicability. To address these limitations, we have devised an explicit SoC planning method that necessitates sparse traffic prior-knowledge, drawing inspiration from the optimal charge depletion behavior. This innovative method strategically determines the average SoC depletion rate for each anticipated driving road segment by integrating theoretical predictions of optimal depletion rate with experienced constraints. Capitalizing on prior knowledge of sparse traffic velocities and road grades, we have developed a hierarchical PEM framework that seamlessly integrates SoC planning — power split. The results of the simulation experiments reveal that the SoC trajectories and fuel consumption generated by this method are in close approximation to theoretically optimal benchmarks. Furthermore, the computational time of this method is in accordance with the demanding real-time requisites of onboard units even if hundreds of miles. Notably, this approach exhibits an enhanced robustness to predictive discrepancies, ensuring reliability and efficacy in dynamic driving cycles.

1. Introduction

Recent advancements in ITS and Vehicle-to-Everything (V2X) now make it feasible to predict forthcoming trip information such as traffic flow velocities, speed limits, and road terrain [1]. The inclusion of these predictive data into the energy management (EM) of Plug-in Hybrid Electric Vehicles (PHEVs), an approach commonly referred to as PEM, has been shown to hold considerable potential for markedly improving fuel economy [2–4].

1.1. Literature review

A substantial body of achievements has been accumulated in the field of PEM through extensive scholarly effort. Hierarchical PEM is a common methodology. The upper layer provides a long-term profile reference by planning the SoC trajectory, while the lower layer controls the power split between the engine and the battery to track the reference, thereby ensuring that the controls approximate the global optimum. This study primarily focuses on the upper layer, SoC planning, which is addressed by mainstream academia through four types of solution.

The first one is based on heuristic or rule-based methods. The discovery that the optimal SoC trajectory tends to display an approximately linear pattern across the overall journeys has inspired the development of linear programming methods. Consequently, numerous scholars have adopted these techniques to implement PEM [5–7], followed by optimization through Model Predictive Control (MPC) [8], Equivalent Consumption Minimization Strategy (ECMS) [9], or Pontryagin's Minimum Principle (PMP) [10] for the completion of power split tasks. Nevertheless, it has been demonstrated that the global optimal consumption profile for SoC is unlikely to be linear [11]. This linearity is manifested only when global driving behaviors are similar. In heterogeneous driving patterns, particularly in conditions alternating between high and low speeds, the global optimal profile is far from linear. A common heuristic idea involves clustering the road sectioned relationship between driving cycles and optimal SoC depletion patterns [12] or establishing a look-up table [13] in offline

* Corresponding author.
E-mail addresses: zhouwei_bit@sina.com (W. Zhou), yilongren@buaa.edu.cn (Y. Ren).

https://doi.org/10.1016/j.energy.2024.133990
Received 13 June 2024; Received in revised form 24 November 2024; Accepted 24 November 2024
Available online 29 November 2024

Nomenclature

α	road grade [/]
$\Delta Q_{dmd,i}$	Q_{dmd}'s variation over BU i [MJ]
ΔSoC_i	SoC's variation over BU i [/]
δ	equivalent inertial coefficient [/]
η_f	final drive efficiency [/]
η_g	gear box efficiency [/]
η_m	traction motor efficiency [/]
η_{apu}	APU efficiency [/]
η_{apu}^{max}	maximum APU efficiency [/]
λ	co-state [/]
$\overline{P_{dmd,bu}^{+}}$	average positive demanded power over a BU [kW]
$\overline{P_{dmd,i}^{+}}$	average positive demanded power over BU i [kW]
$\overline{P_{dmd}^{+}}$	average positive demanded power [kW]
ρ_a	air density [kg/m^3]
A	drag force area [m^2]
C_d	aerodynamic coefficient [/]
f	tire friction coefficient [/]
g	gravity acceleration [ms^{-2}]
m	vehicle cargo mass [kg]
m_f	instantaneous fuel rate [g/s]
$m_{f,idle}$	idle fuel rate [g/s]
P_M	threshold power for APU activation [kW]
$P_{apu,max}$	maximum output power of APU [kW]
P_{apu}	Output power of APU [kW]
P_{brk}	mechanical braking power [kW]
$P_{dmd,e}$	demanded electric power of traction motor in electric mode [kW]
$P_{dmd,h}$	demanded electric power of traction motor in hybrid mode [kW]
P_{wh}	demanded power at driving wheels [kW]
Q_{dmd}	cumulative demanded driving energy [MJ]
Q_{lhv}	lower heating value of fuel [kJ/g]
Q_{nom}	battery nominal capacity [Ah]
R_0	battery ohmic internal resistance [Ω]
SoC_0	initial SoC [/]
SoC_{hb}	highest boundary of SoC [/]
SoC_{lb}	lowest boundary of SoC [/]
sq_e	instantaneous CDR of pure electric mode [J^{-1}]
sq_h	instantaneous CDR of hybrid electric mode [J^{-1}]
V	vehicle velocity [m/s]
V_{oc}	battery open circuit voltage [V]

phases to support rapid query by online cycles for planning nearly optimal trajectories. Nevertheless, this method is only applicable to driving cycles similar to those in the offline phase [12] or to commuter vehicles with fixed routes [13].

Heuristic or rule-based methods may not be optimal since humans tend to be inspired by only a small part of driving cycles rather than the universe, limiting the generalizability of these methods. Therefore, some scholars have turned to optimization-based approaches for SoC planning, using methods like Dynamic Programming (DP) [14,15], PMP [16], Particle Swarm Optimization (PSO) [17], and Monte Carlo Tree Search (MCTS) [18], etc. These optimization methods are primarily constrained by two factors. Firstly, accurate driving cycles or traffic information of energy consumption are the necessary prior-knowledge for optimization. Using the representative driving cycles with fixed routes [15] or data-driven methods [14,17] to predict are two typical ideas, but the optimization heavily relies on the matching degree between prior information and actual driving cycles, which is rarely considered in the literature. Secondly, the computational burden is heavy, and then limits the practical application. For instance, DP, which necessitates traversing the entire computational space, often leads to a conflict between real-time performance and optimization, rendering it nearly impossible to achieve real-time trajectory planning that is close to optimal.

To address issues with real-time performance, a cutting-edge research idea employs Deep Neural Network (DNN) technology to learn real-time inference of optimal SoC trajectories. The most common idea involves the collection of a substantial number of driving cycles, then globally optimizing the SoC trajectory using offline methods such as DP [19] or PMP [20], and finally training of the optimal planning solutions using deep learning [21] or reinforcement learning [22] techniques to develop well-trained inference models. During the online phase, the NN model infers the SoC trajectory in real-time based on the predicted prior driving cycles. Nevertheless, this methodology is encumbered by the considerable computational load associated with its training phase, as well as the necessity to amass expansive datasets, thereby imposing significant demands on the hardware. Furthermore, the issue of Out-of-Distribution (ODD) generalization [23] remains unresolved well.

The analytical method is a challenging but highly promising solution due to the optimization and real-time performance. These methods often derive nearly optimal fully or semi-explicit solutions by simplifying optimization goals, reducing constraint limits, and decreasing the degree of nonlinearity. Kuchly et al. [24] derived an analytical solution to the optimal control problem and used light cartographic information to address problematic cases. However, this approach requires high granularity in map information. To address the issue, a constrained eco-routing strategy for hybrid vehicles based on semi-analytical EMS was proposed [25], allowing for the rapid determination of SoC's linear consumption in sparse road segmentation. Nevertheless, the challenge remains that real-time performance still fails to meet on-board requirements. Zhou et al. [26] were inspired by the optimal linear consumption laws of SoC trajectories on the energy domain and conducted energy-based analytical SoC planning after splitting future driving cycles. Simulations demonstrated nearly optimal optimization performance, but only in special hilly cycles. Furthermore, and the heuristic laws have not been formally proved. Subsequently, Zhou et al. [27] explored further in optimal SoC consumption behaviors. In particular, a single-objective explicit optimization equation based on the PMP decoded the optimal charge depletion behavior and derived the optimal SoC planning trajectories on the energy domain. Although it has good real-time performance, the design of PEM based on the analytical SoC planning on the spatial domain has yet to be effectively realized. However, this path has provided significant insights, summarizing two major unresolved issues: (1) Translation of SoC planning from the energy domain to the spatial domain to support the practical design of PEM; (2) Reduction of the reliance on high-granularity traffic information while still maintaining optimization, which helps reducing dependence on high-cost ITS, and accelerating the deployment of PEM. The methodology delineated within this manuscript addresses both aforementioned issues while concurrently securing optimal refinement, real-time operability, and minimal reliance on preliminary data — a triad of performance metrics that present methodologies struggle to realize simultaneously.

1.2. Motivation and contribution

As summarized above, existing methods often struggle to balance optimization and real-time capabilities, and typically require accurate detailed predictive information, significantly increasing the deployment complexity of PEM systems. Inspired by the literature [27], optimal charge depletion behavior on the energy domain has been explicitly analyzed. It provides a basis for transforming the SoC planning from the energy domain to the spatial domain, thus integrating it into the EMS. Building upon [27], we further offer a hierarchical PEM framework and an explicit SoC planning solution inspired by the optimal behavior.

Our contribution lies in the three folds:

1. We propose a method to transform optimal charge depletion from the energy domain to the spatial domain, eliminating the dependency on high-granularity prior-knowledge from the perspective of experienced boundary constraints on the spatial domain, thus providing insights for SoC planning within PEM.
2. To our best knowledge, this is the first study to design an analytical SoC planning method inspired by the optimal charge depletion behavior that requires only sparse predictive information to achieve trajectories close to optimal.
3. A hierarchical real-time PEM framework was constructed, which, according to simulation results, aligns closely with near-global optimal fuel consumption outcomes. This framework is characterized by low computational demands, indicating significant promise for onboard implementation in hybrid electric vehicles.

1.3. Material organization

The remainder of this paper is organized as follows: Section 2 summarizes the formulation of the optimal EM problem and optimal charge depletion on the energy domain. Section 3 presents an explicit SoC planning method based on the spatial-domain charge depletion rate inspired by the optimal behaviors. Section 4 introduces a hierarchical real-time PEM framework for SoC planning and power split. Section 5 validates the proposed PEM using a high-fidelity co-simulation platform, evaluating SoC planning, fuel consumption, real-time performance, and robustness. Finally, main conclusions are drawn in Section 6.

2. Optimal charge depletion behavior

The subject of this study is a plug-in hybrid electric bus with the series powertrain configuration as illustrated in Fig. 1. The major task of the EM strategy is to maximize fuel economy while meeting the demanded driving power [28]. To achieve this goal, an optimal EM problem is formulated based on the PMP, and the optimal charge depletion on the energy domain is reviewed in the following.

2.1. Optimal energy management problem formulation

2.1.1. Objective function

The objective function represents the sum of instantaneous fuel consumption over the entire journey:

$$J\left(P_{apu}(t)\right)=\int_{t_0}^{t_f}\dot{m}_f\left(P_{apu}(t)\right)dt=\int_{t_0}^{t_f}\frac{P_{apu}(t)}{\eta_{apu}(P_{apu}(t))Q_{lhv}}dt \tag{1}$$

where P_{apu} is the control input of the EM. Since the APU can operate decoupled from the vehicle drivetrain, it can function along its maximum efficiency curve, as shown in Fig. 2.a. Therefore, the instantaneous fuel rate can be calculated by the maximum efficiency according to:

$$\dot{m}_f\left(P_{apu}(t)\right)=\frac{P_{apu}(t)}{\eta_{apu}^{max}(P_{apu}(t))Q_{lhv}} \tag{2}$$

Table 1
Values of related vehicle parameters.

Parameter	Value	Parameter	Value
η_f	0.97	f	0.012
η_g (at 1st gear)	0.93	η_g (at 2nd gear)	0.95
m	14,500	ρ_a	1.225
A	7.67	C_d	0.8
δ (at 1st gear)	1.1268	δ (at 2nd gear)	1.0125

The instantaneous fuel rates obtained using Eq. (2) are visualized in Fig. 2.b, which also shows that the experimental data is fitted with very good accuracy by a 3-order polynomial function expressed as:

$$\dot{m}_f\left(P_{apu}(t)\right)=m_{f,idle}+k_1P_{apu}(t)+k_2P_{apu}^2(t)+k_3P_{apu}^3(t) \tag{3}$$

where the fitting coefficients are $k_1=7.3212\times10^{-5}$, $k_2=-4.8287\times10^{-10}$, $k_3=4.1035\times10^{-15}$; and $m_{f,idle}$ is the idle fuel consumption rate, valued at 0.0808 g/s. Note that the 3-order fit is a fundamental condition for analytical analysis [27].

2.1.2. State equation

A widely used battery model that represents the battery as an electrical circuit comprised of a voltage source and a purely ohmic impedance is adopted [30]. In the proposed model, the SoC of the battery emerges as the sole state variable requiring optimization, with its dynamics dictated by Eq. (4). It is important to note that the impact of temperature on battery parameters is overlooked, predicated on the assumption of an adequately robust thermal management.

$$\begin{aligned}\dot{SoC}(t)&=-\frac{V_{oc}\left(SoC(t)\right)-\sqrt{V_{oc}^2(SoC(t))-4(P_{dmd}(t)-P_{apu}(t))R_0(SoC(t))}}{2R_0\left(SoC(t)\right)Q_{nom}}\\&\equiv f\left(SoC(t),P_{apu}(t)\right)\end{aligned} \tag{4}$$

where P_{dmd} is the electric power demanded by the traction motor, which can be calculated using the following energy-oriented model [29]:

$$\begin{cases}P_{dmd}(t)=\begin{cases}\frac{P_{wh}(t)}{\eta_m(t)\eta_g(t)\eta_f} & ,P_{wh}(t)\geq0\\\left(P_{wh}(t)-P_{brk}(t)\right)\eta_m(t)\eta_g(t)\eta_f & ,P_{wh}(t)<0\end{cases}\\P_{wh}(t)=\left(\delta m\dot{V}(t)+fmgcos\alpha(t)+0.5\rho_aC_dAV^2(t)+mgsin\alpha(t)\right)V(t)\end{cases} \tag{5}$$

where P_{brk} is the mechanical braking power determined by a maximum energy-recovery regenerative braking strategy [31]. Values of related vehicle parameters are listed in Table 1.

2.1.3. System constraints

First of all, a terminal state constraint as expressed by Eq. (6) is needed to prevent over-discharge of the battery. In all the simulations of this study, SoC_f is set as 0.3. We note that the value of SoC_f will not influence the analytical derivation in the following section.

$$SoC(t_f)=SoC_f \tag{6}$$

Moreover, some state and control constraints due to physical limits or safety concerns are required to be satisfied:

$$\begin{cases}0\leq P_{\text{apu}}(t)\leq P_{\text{apu,max}}\\SoC_{lb}\leq SoC(t)\leq SoC_{hb}\\P_{b,min}(t)\leq P_b(t)\leq P_{b,max}(t)\end{cases} \tag{7}$$

where $P_{b,min}$ and $P_{b,max}$ represent the charging and discharging power capability of the battery, which is respectively restricted by the battery's upper and lower cut-off voltages.

2.2. Optimal charge depletion on the energy domain

Following the research outlined in [27], the relationship between the rate of decline of the SoC and the value of the P_{dmd}^+ (positive value

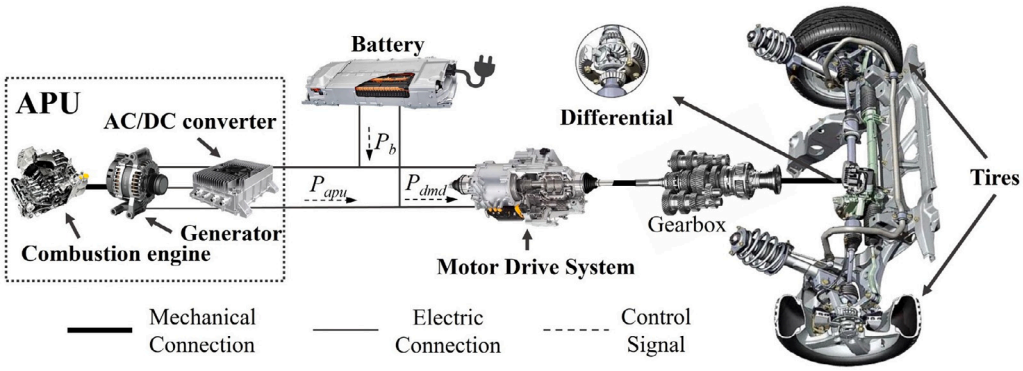

Fig. 1. Configuration scheme of the series PHEV. The primary components and parameters of the power system are as follows: the nominal power of engine-generator set (APU) is 75 kW; the nominal power of permanent magnet synchronous motor is 130 kW, and the peak power is about 170 kW; the nominal energy capacity of lithium-ion battery pack is 140 Ah (59 kWh). The gearbox has two gears whose shifting is controlled by velocity-dependent rules as presented in [29].

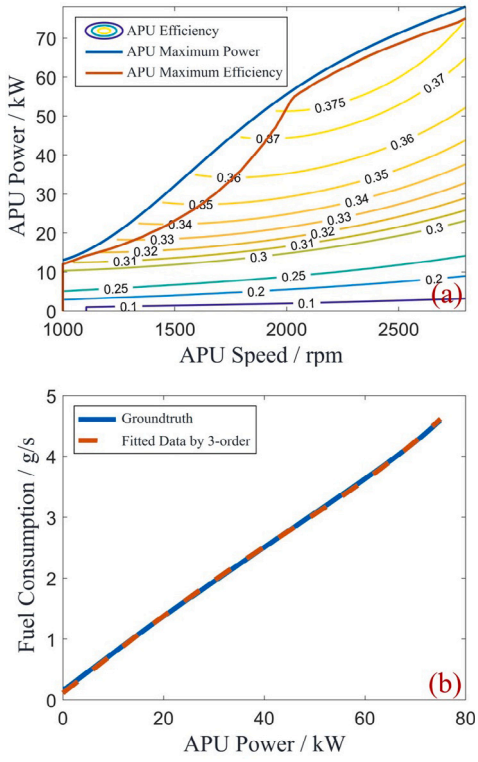

Fig. 2. (a) Quasi-static efficiency map and maximum efficiency line of the APU system; (b) Instantaneous fuel rates for the maximum efficiency line. (For interpretation of the references to color in this figure legend, the reader is referred to the web version of this article.)

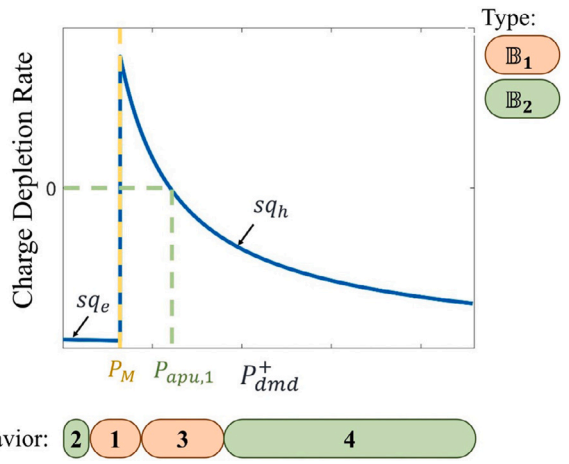

Fig. 3. Relationship of CDR and P^+_{dmd} on the energy domain [27]. The approximate region of the four optimal charge depletion behaviors related to P^+_{dmd} are illustrated as the bottom rounded square. The type $\mathbb{B}_1$ includes behaviors 1 and 3, and $\mathbb{B}_2$ includes behaviors 2 and 4. P^+_{dmd} governed by behavior 1 is far less than P_M; P^+_{dmd} governed by behavior 2 is around P_M; P^+_{dmd} governed by behavior 3 is around $P_{apu,1}$; P^+_{dmd} governed by behavior 4 is far greater than $P_{apu,1}$.

of P_{dmd}) on the energy domain, termed the Charge Depletion Rate (CDR), is illustrated in Fig. 3 and expressed as:

$$CDR_{dri} = \begin{cases} sq_h = -\frac{P_{dmd,h}-P_{apu,1}}{V_{oc}Q_{nom}P_{dmd,h}}\left(1+\frac{R_0(P_{dmd,h}-P_{apu,1})}{V_{oc}^2}\right) & , P^+_{dmd} > P_M \\ sq_e = -\frac{1}{V_{oc}Q_{nom}}\left(1+\frac{R_0P_{dmd,e}}{V_{oc}^2}\right) & , P^+_{dmd} \le P_M \end{cases} \quad (8)$$

where, when P^+_{dmd} exceeds the threshold P_M, the APU is engaged, and the optimal CDR_{dri} is sq_h; otherwise, with the APU off, the optimal CDR_{dri} is sq_e. It is demonstrated that once the APU is activated, it operates near $P_{apu,1}$. $P_{apu,1}$ approximates constant 60 kW. P_M is inversely related to $Q_{dmd,tot}$, providing insights for the design of an energy-based PEM framework. During regenerative braking $P_{dmd} < 0$, which essentially utilizes a pure electric mode, $CDR_{reg} = -sq_e$. Thus, the explicit relationship between CDR and P_{dmd} can be summarized as:

$$CDR = f^*(P_{dmd}) \quad (9)$$

where f^* represents the optimal functional relationship between CDR and P_{dmd}.

Further, four behaviors are identified, and the literature [27] based on their sensitivity to CDR relative to P_{dmd}, categorizes them into two modes requiring varying granularity of P_{dmd} prior-knowledge. This study delineates them based on the regions of P_{dmd} into two types: $\mathbb{B}_1$, one occurs near the breakpoint around P_M and the large slope near $P_{apu,1}$; $\mathbb{B}_2$, another occurs near the two end areas dominated by either electric or hybrid mode. Notably, $\mathbb{B}_2$ is interrupted by $\mathbb{B}_1$. When the P_{dmd} of a road section is in the $\mathbb{B}_1$ region, the minor changes of it can lead to drastic shifts in CDR. Therefore, $\mathbb{B}_1$ and $\mathbb{B}_2$ require high granularity in the distribution of P_{dmd} and low granularity in the P^+_{dmd} (average P_{dmd}) respectively.

However, this SoC planning methodology, based on precise driving energy predictions, struggles to meet the terminal value constraints of

SoC in online PEM. Consequently, it is necessary to shift to the spatial domain where can be more accurately estimated. Moreover, obtaining high-granularity P_{dmd} distributions can be challenging, significantly increasing the construction costs and data interaction difficulties for ITS. It is therefore imperative to lessen the reliance on highly granular data by refining our prediction strategies.

3. Method for state-of-charge planning

3.1. Prediction of optimal charge depletion rate

Typically, ITS can only provide sparse road sectioned traffic information [32], such as flow velocity and average road slope. Therefore, our research bases on road sectioned traffic prior information assumption, moreover, consistent traffic and road conditions within each section but significant differences between the adjacent [26]. Thus, the instantaneous optimal relationship can be extended to the macroscopic scale:

$$CDR = f^*(P_{dmd}) \Rightarrow \overline{CDR} \approx f^*(\overline{P_{dmd}}) \tag{10}$$

Assuming the target route is divided into N road sub-sections with different average driving forces, for a given road section i, the following relationship holds:

$$\frac{\Delta SoC_i}{\Delta Q_{dmd,i}} = \frac{\Delta SoC_i}{\bar{F}_{drive,i} s_i} = \frac{\overline{k}_i^*}{\bar{F}_{drive,i}} = \overline{CDR}_i \tag{11}$$

where $\bar{F}_{drive,i}$ is the average driving force over i_{th} road section, representing the average driving energy on the spatial domain of that road sub-section and s_i is the distance of i_{th} travel segment; $\frac{\Delta SoC_i}{s_i}$ is the rate of decline, $\overline{k}_i^*$, of the optimal SoC trajectory, which is the charge depletion rate on the spatial domain.

Drawing upon the piecewise linear interdependence between SoC and Q_{dmd}, the relationship between any two road sub-sections can be derived as:

$$\frac{\bar{k}_i}{\bar{k}_j} = \frac{\bar{F}_{drive,i}\overline{CDR}_i}{\bar{F}_{drive,j}\overline{CDR}_j} \tag{12}$$

According to the law of energy conservation, for any two road sections:

$$\begin{cases} \bar{\eta}_d \bar{F}_{drive,i} s_i = \bar{F}_{road,i} s_i + \Delta E_{v,i} + \Delta E_{mb,i} \\ \bar{\eta}_d \bar{F}_{drive,j} s_j = \bar{F}_{road,j} s_j + \Delta E_{v,j} + \Delta E_{mb,j} \end{cases} \tag{13}$$

where $\bar{\eta}_d$ is the average efficiency of the drivetrain; $\bar{F}_{road}$, ΔE_v, and ΔE_{mb} respectively represent the average road resistance, change in kinetic energy, and energy loss due to mechanical braking. Combining Eqs. (12) and (13) further concludes that:

$$\frac{\bar{k}_i}{\bar{k}_j} = \frac{\bar{F}_{road,i}\overline{CDR}_i}{\bar{F}_{road,j}\overline{CDR}_j} \cdot \frac{\frac{\bar{F}_{road,j} s_j}{\bar{F}_{road,j} s_j + \Delta E_{v,j} + \Delta E_{mb,j}}}{\frac{\bar{F}_{road,i} s_i}{\bar{F}_{road,i} s_i + \Delta E_{v,i} + \Delta E_{mb,i}}} \tag{14}$$

Assuming that the majority of the driving energy on each road section is consumed by road resistance, we approximate the following:

$$\frac{\bar{k}_i}{\bar{k}_j} \approx \frac{\bar{F}_{road,i}\overline{CDR}_i}{\bar{F}_{road,j}\overline{CDR}_j} \tag{15}$$

This assumption is based on two reasons. Firstly, after refining the segmentation of the road sections, the differences in initial and terminal velocities for each road section are relatively small, allowing the kinetic energy change ΔE_v to be negligible. Furthermore, in typical driving cycles, the maximum energy recovery strategy employed in regenerative braking allows most of the energy to be recuperated to the battery, thus ΔE_{mb} is also small.

The average road resistance in Eq. (15) can be estimated using the average velocity $\bar{v}$ and the average road slope $\bar{\alpha}$ for each road section:

$$\bar{F}_{road} = \frac{1}{2}\rho_a C_d A \bar{v}^2 + mgsin\bar{\alpha} + mgfcos\bar{\alpha} \tag{16}$$

To ensure constraints at two boundary points value of SoC, the SoC must satisfy:

$$\sum_{i=1}^{N_{dri}} \Delta SoC_{drive,i} = SoC_f - SoC_0 + \sum_{j=1}^{N_{reg}} \Delta SoC_{reg,j} \tag{17}$$

where N_{dri}, ΔSoC_{dri}, and N_{reg}, ΔSoC_{reg} respectively denote the total number of road sections and the SoC variation dominated by driving and regenerative braking, respectively. The ΔSoC_{reg} can be calculated as:

$$\Delta SoC_{reg,i} = \bar{\eta}_d \bar{F}_{road,i} s_i \overline{CDR}_{reg} \tag{18}$$

where $\overline{CDR}_{reg}$ ($\approx (Q_{nom}\bar{V}_t)^{-1} = const$, $\bar{V}_t$ is corresponding to the average terminal voltage of the battery in road sections in which SoC rising) denotes the CDR value during regenerative braking. Integrating Eqs. (15) and (16) into Eq. (17) derives the k values corresponded of road sections governed by driving and regenerative braking:

$$\begin{cases} \bar{k}_{dri,i} = \overline{F}_{road,i}\overline{CDR}_i \frac{SOC_f - SOC_0 + \sum_{j=1}^{Nreg} \Delta SOC_{reg,j}}{\sum_{i=1}^{Ndri} \overline{F}_{road,i} s_i \overline{CDR}_i} \\ \bar{k}_{reg,i} = \frac{\Delta SOC_{reg,i}}{s_i} \end{cases} \tag{19}$$

The SoC end value of each road section is:

$$SoC_i = SoC_0 - \sum_{j=1}^{i} \Delta SoC_j = SOC_0 - \sum_{j=1}^{i} \bar{k}_i s_i \tag{20}$$

Sequentially connecting a series of nodes (s_i, SOC_i) constructs a piecewise linear reference SoC trajectory on the spatial domain.

Only $\overline{CDR}_i$ remains unknown. According to Section 2, the prediction of $\overline{CDR}_i$ requires using charge depletion behaviors of different road sections to choose data of diverse granularity prior information. Table 2 quantifies four types of power boundaries of the charge depletion behaviors, while performing PEM, enabling quick determination of the optimal charge depletion mode, $\mathbb{B}_1$ or $\mathbb{B}_2$, directly based on the predicted average power $\widehat{P^+_{dmd}}$ of road sections.

Then it is necessary to predict the value of P_M to determine each behavior intervals. Although a negative correlation trend exists between P_M and the total driving energy demand $Q_{dmd,tot}$ [27], the fitting curve does not accurately predict the value of P_M. Based on the relationship between the energy of the APU, the battery, and the total driving energy:

$$Q_{dmd,tot} = Q_{bat} + P_{apu,1}\Delta t_{apu} \tag{21}$$

In this equation, apart from the duration Δt_{apu} that the APU is active, other parameters can be estimated with relative accuracy, thus Δt_{apu} can be calculated. The P_M will determine the size of Δt_{apu}. By combining the historical demand power trajectory with the future predicted power, the P_M value is predicted by traversal satisfying the conditions that the total time in which P_{dmd} is greater than P_M is equal to Δt_{apu}.

The total energy demand $Q_{dmd,tot}$ consists both of historical accumulated energy consumption and future predicted energy consumption:

$$\hat{Q}_{dmd,tot} = \underbrace{\int_{t_0}^{t_{cur}} P_{dmd}\,dt}_{\text{energy consumption}} + \underbrace{\frac{\sum_{i=1}^{N_{remain}} \bar{F}_{road,i} s_i}{\bar{\eta}_d}}_{\text{energy requirement}} \tag{22}$$

where t_0 and t_{cur} represent the departure and current time, respectively, and N_{remain} indicates the number of remaining road sections.

Finally, the prediction of $\overline{CDR}$ needs to select different granularity prediction information according to the power interval of $\widehat{P^+_{dmd}}$, to ensure good predictive accuracy while minimizing reliance on high-granularity predictive information.

For the road sections governed by mode $\mathbb{B}_2$, which requires lower granularity of prediction information, only the average power $\overline{P^+_{dmd}}$ prediction information is needed:

$$\overline{P^+_{dmd,i}} = \frac{\bar{F}_{road,i}\bar{v}_i}{\bar{\eta}_d} \tag{23}$$

Table 2
Quantification interval of the charge depletion behaviors.

Interval (kW)	$0 \le P_M < P_{apu,1}$	$P_{apu,1} \le P_M < P_{apu,1}+20$	$P_{apu,1}+20 \le P_M \le P_{apu,max}$
Behavior '①'	$P_M-15 \sim P_M+15$	$P_M-15 \sim P_{apu,1}+20$	$P_M-15 \sim P_M+15$
Behavior '②'	$0 \sim P_M-15$		
Behavior '③'	$P_M+15 \sim P_{apu,1}+20$		/
Behavior '④'	$P_{apu,1}+20 \sim P_{apu,max}$		$P_M+15 \sim P_{apu,max}$
$\mathbb{B}_1$	$P_M-15 \sim P_{apu,1}+20$		$P_M-15 \sim P_M+15$
$\mathbb{B}_2$	$0 \sim P_M-15, P_{apu,1}+20 \sim P_{apu,max}$		$0 \sim P_M-15, P_M+15 \sim P_{apu,max}$

where $\overline{CDR_i}$ can be calculated using Eq. (8) based on $\overline{P^+_{dmd,i}}$.

For road sections where the average power falls within $\mathbb{B}_1$, according to the $CDR-P^+_{dmd}$ curve (see Fig. 3), the probability distribution $\Pr(P_{dmd,i})$ of P^+_{dmd} is transformed into a probability distribution $\Pr(CDR_i)$ of CDR:

$$\Pr\left(CDR_i\right) = f^*(\Pr\left(P_{dmd,i}\right)) \tag{24}$$

Then CDR's mathematical expectation $E(CDR) = \sum CDR \times \Pr(CDR)$ is calculated to determine the predicted $\widehat{CDR}$ corresponded for the road section.

3.2. Experienced boundary constraints

However, in many cases, ITS may not provide accurate detailed distribution information related to P_{dmd}, such as single-vehicle energy consumption and road elevation data. To further minimize the reliance on high-accuracy predictive information in SoC planning, this study predicts the boundary of optimal rate of decline from the standpoint of optimal charge depletion mechanics on the spatial domain, aiming to reduce optimization degradation caused by the lack of high-granularity prior-information.

Based on the SoC state equation (Eq. (4)), the CDR on the spatial domain is derived:

$$\begin{aligned} k^* &= \frac{S\dot{o}C}{\dot{s}} \\ &= -\frac{V_{oc}(SoC(t)) - \sqrt{V^2_{oc}(SoC(t)) - 4R_0(SoC(t))(P_{dmd}(t)-P_{apu}(t))}}{2R_0(SoC(t))Q_{nom}v(t)} \end{aligned} \tag{25}$$

where k^* is influenced by the dynamic variations in parameters such as $V_{oc}(SoC(t))$, $R_0(SoC(t))$, $P_{dmd}(t)$, $P_{apu}(t)$, and $v(t)$, with each parameter affecting k^* to different extents. To facilitate sensitivity analysis, the 1-order Taylor expansion approximation of the square root term at $P_{dmd}(t)-P_{apu}(t)=0$ in the numerator of Eq. (25) is conducted:

$$\sqrt{V^2_{oc} - 4R_0(P_{dmd}-P_{apu})} \approx V_{oc} - \frac{2R_0}{V_{oc}}(P_{dmd}-P_{apu}) \tag{26}$$

Fig. 4 demonstrates the comparison between the 1-order Taylor expansion of $\sqrt{V^2_{oc} - 4R_0(P_{dmd}-P_{apu})}$ and the original values within the domain defined for $P_{dmd}-P_{apu}$, thus validating the accuracy of the approximation. The perturbation analysis of various parameters on the k^* is as follows:

(1) $V_{oc}(SoC(t))$:

$$\begin{aligned} \xi(V_{oc}) &= \left|\frac{\hat{k}^*-k^*}{k^*}\right| \\ &= \frac{-\frac{(V_{oc}+\Delta V_{oc})-\sqrt{(V_{oc}+\Delta V_{oc})^2-4R_0(P_{dmd}-P_{apu})}}{2RQ_{nom}v} + \frac{V_{oc}-\sqrt{V^2_{oc}-4R_0(P_{dmd}-P_{apu})}}{2RQ_{nom}v}}{-\frac{V_{oc}-\sqrt{V^2_{oc}-4R_0(P_{dmd}-P_{apu})}}{2RQ_{nom}v}} \\ &\approx -\frac{\Delta V_{oc}}{V_{oc}+\Delta V_{oc}} \end{aligned} \tag{27}$$

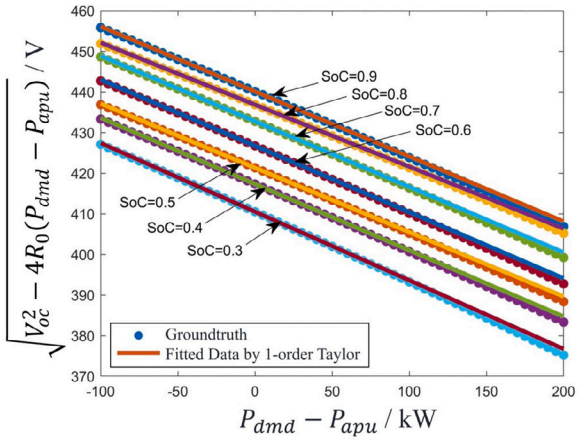

Fig. 4. Comparison between the 1-order Taylor approximation of $\sqrt{V^2_{oc} - 4R_0(P_{dmd}-P_{apu})}$ and the original function values.

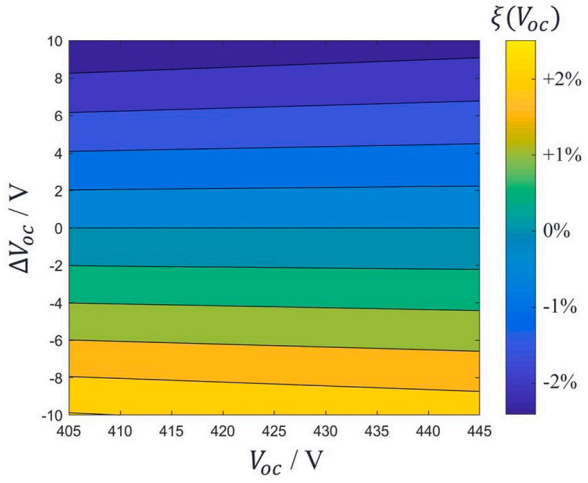

Fig. 5. Relationship between $\xi(V_{oc})$, V_{oc}, and ΔV_{oc}. (For interpretation of the references to color in this figure legend, the reader is referred to the web version of this article.)

Fig. 5 illustrates the relationship among the change rate $\xi(V_{oc})$ concerning both the open-circuit voltage V_{oc} and the voltage variation ΔV_{oc}. It is evident that within the defined domain for V_{oc} and ΔV_{oc}, as the absolute value of ΔV_{oc} increases, the absolute value of $\xi(V_{oc})$ also increases, yet overall, k^* is minimally influenced by changes in V_{oc}. Given that the actual rate of change in battery voltage ΔV_{oc} is minimal, the impact of V_{oc} on k^* can be entirely disregarded.

(2) $R_0(SoC(t))$:

$$\xi(R_0) = \left|\frac{\hat{k}^* - k^*}{k^*}\right| = \frac{\frac{V_{oc}-\sqrt{(V_{oc}^2-4(R_0+\Delta R_0))(P_{dmd}-P_{apu})}}{2(R+\Delta R)Q_{nom}v} + \frac{V_{oc}-\sqrt{V_{oc}^2-4R_0(P_{dmd}-P_{apu})}}{2RQ_{nom}v}}{-\frac{V_{oc}-\sqrt{V_{oc}^2-4R_0(P_{dmd}-P_{apu})}}{2RQ_{nom}v}} \approx 0 \tag{28}$$

The impact of the internal resistance R_0 on k^* can likewise be considered negligible.

(3) $P_{apu}(t)$: The output power range of the APU described in this study spans from 0 to $P_{apu,max}$. According to the optimal control analysis (Eq. (8)), the optimal output power of the APU is either 0 or $P_{apu,1}$. Given the power response hysteresis inherent to actual APUs, minor instances may occur where the actual APU output power lies in $(0, P_{apu,1})$; however, these instances are generally negligible for long-range driving cycles.

Consequently, it is sufficient to consider the dynamics of k^* in relation to $P_{dmd}(t)$ and $v(t)$. To summarize, the k^* on the spatial domain concerning P_{dmd} and v is expressed as a function:

$$k^*(P_{dmd}, v) = \begin{cases} -\frac{V_{oc}-\sqrt{V_{oc}^2-4R_0(P_{dmd}(t)-0)}}{2R_bQ_{nom}v(t)} & ,0 < P_{dmd} < P_M \\ -\frac{V_{oc}-\sqrt{V_{oc}^2-4R_0(P_{dmd}(t)-P_{apu,1})}}{2R_bQ_{nom}v(t)} & ,P_{dmd} \geq P_M \end{cases} \tag{29}$$

For an example with $V_{oc} = \overline{V_{oc}}$, $R_0 = \overline{R_0}$, and $P_M = 40kW$, the relationship between the $\overline{k^*}$ and P_{dmd}, v is depicted in Fig. 6. In the dimension of P_{dmd}, a discontinuity appears in $\overline{k^*}$ at $P_{dmd} = P_M$, with $\overline{k^*}$ decreasing as P_{dmd} increases on either side of P_M. In the dimension of v, within the interval $[0, P_M] \cup [P_{apu,1}, P_{apu}^{max}]$, k^* increases with increasing v, and decreases with increasing v within the interval $[P_M, P_{apu,1}]$. By defining P_{dmd}, v, and P_M, $\overline{k^*}$ can be determined. Generally, for behaviors '②', '③', and '④', the APU is mostly in either an off or on state, and $\overline{k^*}$ will approximate $\overline{k^*}(\overline{P_{apu}^*})$; however, for the charge depletion behavior '①' on the energy domain, due to fluctuating power demands around the value P_M, the APU may frequently switch between on and off states. In the absence of high-granularity statistical distribution of P_{dmd}, it is challenging to determine specific predicted values of $\overline{k^*}$. At this point, the range of $\overline{k^*}$ values lie between the APU being off and on:

$$-\frac{V_{oc}-\sqrt{V_{oc}^2-4R_0(\overline{P_{dmd}}-0)}}{2R_0Q_{nom}\bar{v}} = \bar{k}^*(P_{apu}=0) \leq \bar{k}^* \leq \bar{k}^*(P_{apu}=P_{apu,1}) = -\frac{V_{oc}-\sqrt{V_{oc}^2-4R_0(\overline{P_{dmd}}-P_{apu,1})}}{2R_0Q_{nom}\bar{v}} \tag{30}$$

Therefore, the predicted range of $\overline{k^*}$ for each road section can be identified, as shown in Fig. 7. The black solid line corresponds to Eq. (29). For the road sections where $\overline{P_{dmd}}$ governed by behaviors '②', '③', and '④', the curve's continuity and clustering segmentation assumptions hold, $\overline{k^*}$ approximates $k^*(\overline{P_{apu}^*}, \bar{v})$. Hence, small range constraints on k^* can be set to minimize deviation in the predicted $\overline{k^*}$:

$$k^*(\overline{P_{apu}^*}, \bar{v}) - k_{low,b} < \overline{k^*} < k^*(\overline{P_{apu}^*}, \bar{v}) + k_{up,b} \tag{31}$$

For road sections under behavior '①' at $\overline{P_{dmd}}$, due to the curve's discontinuity, $\overline{k^*}$ may significantly differ from $k^*(\overline{P_{apu}^*}, \bar{v})$. On the left side of P_M, k^* on both adjacent sides is higher than itself, hence $\overline{k^*}$ generally is more than $k^*(\overline{P_{apu}^*}, \bar{v})$, hence $k_{low,b} = 0$; since $\overline{P_{dmd}} < P_M$, these road sections predominantly operate in pure electric mode, aiming to avoid energy transfer losses from APU charging the battery, thus $k_{up,b} = -k^*(\overline{P_{apu}^*}, \bar{v})$. On the right side of P_M, all other areas have k^* less than itself, so $\overline{k^*}$ is definitively less than $k^*(\overline{P_{apu}^*}, \bar{v})$, and $k_{up,b} = 0$; for road sections within $[P_M, P_{apu,1}]$ at $\overline{P_{dmd}}$, $\overline{k^*} > 0$, with the APU charging the battery to meet the both end-point constraints of SoC, therefore $k_{low,b} = k^*(\overline{P_{apu}^*}, \bar{v})$.

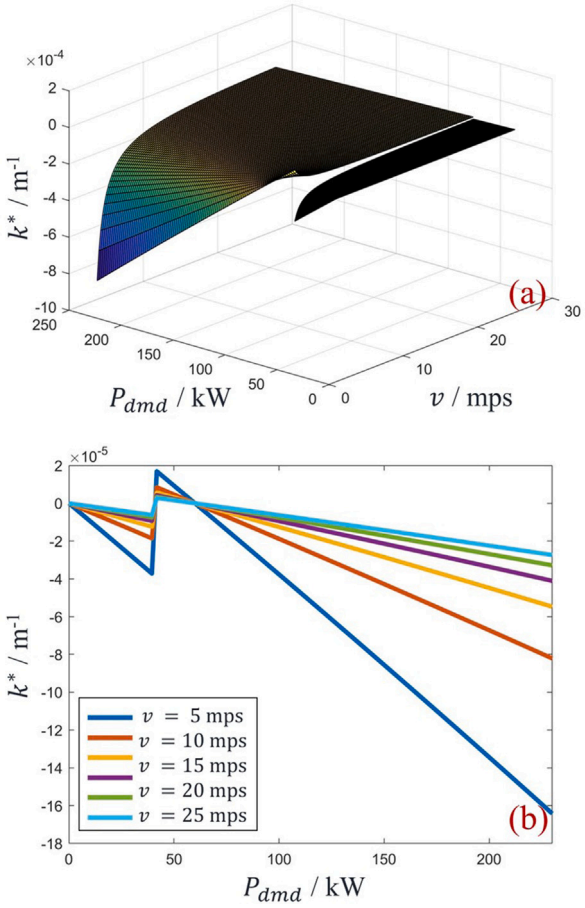

Fig. 6. (a) Relationship of k^* with P_{dmd} and v; (b) Relationship of k^* and P_{dmd} within different v. (For interpretation of the references to color in this figure legend, the reader is referred to the web version of this article.)

3.3. State-of-charge planning

Based on the analysis above, a piecewise linear online SoC planning algorithm is proposed, the pseudo-code of which is presented in **Algorithm 1**.

3.3.1. Algorithm for state-of-charge trajectory planning

The inputs to the algorithm include predicted data information obtained from ITS, comprising total mileage of the road ahead, road section length, traffic flow speed, road gradient, and essential parameters of the vehicle (as shown in Table 1). The output is a piecewise linear reference trajectory of the SoC on the spatial domain. It can be mainly divided into the following 7 steps:

- The first step (line 1) uses an ordered sample clustering algorithm [33] to segment the road based on traffic road sections and slope information, matching the road length of the sub-section s_i, average traffic speeds $\overline{v_i}$, average gradients $\overline{\alpha_i}$, and the number of road sub-sections N in the input data.
- Subsequently, the CDR curve (including sq_e and sq_h segments) is computed based on the average power of the road sub-sections $\overline{P_{dmd}}$ and the predicted $\hat{P}_M$, as in the line 2.
- The next step predicts the charge depletion behavior for each road sub-section based on the relative relationship of $\overline{P_{dmd}}$ with P_M and $P_{apu,1}$, as shown in lines 3 ~ 5.

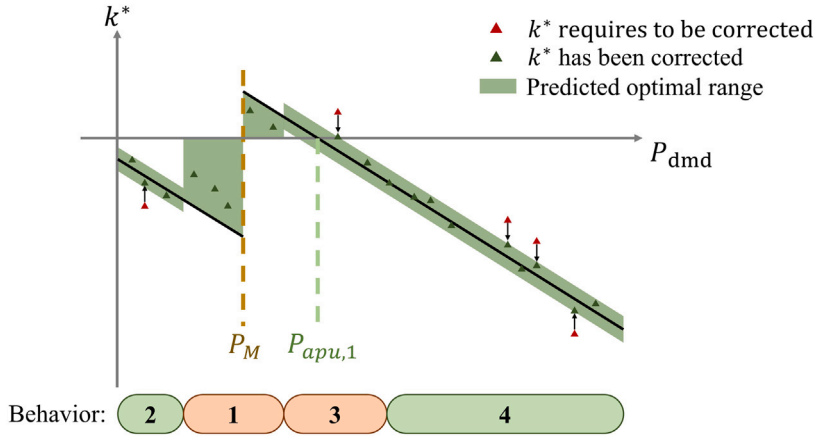

Fig. 7. Schematic of boundary constraints of $\overline{k^*}$.

Algorithm 1 Piecewise Linear State-of-Charge Trajectory Planning

Input: ITS prior data: total length of the global route s, average traffic flow velocity $\overline{v_i}$ for each road section, road sub-section length s_i, road gradient α_i; vehicle parameters.

Output: Reference SoC trajectory on the spatial domain.

1: s_i, $\overline{v_i}$, $\overline{\alpha_i}$,N ← **Global Route Segmentation** by ordered sample clustering;
2: CDR **Curve Estimation** based on Eq. (8);
3: **for** $i = 1 : N$ **do**
4: **Behavior Determination** of each road section based on Tab. 2;
5: **end for**
6: **for** $i = 1 : N$ **do**
7: $\overline{CDR_i}$ **determination** based on Eq. (23) and Eq. (24);
8: **end for**
9: **for** $i = 1 : N$ **do**
10: $\overline{k}_i^*$ **determination** based on Eq. (19);
11: **end for**
12: **for** $i = 1 : N$ **do**
13: **if** the behavior of the i_{th} section is '②', '③', or '④' **then**
14: $\bar{k}_i = min(k_{max}, max(k_{min}, \bar{k}_i))$ based on Eq. (31);
15: **end if**
16: **end for**
17: **for** $i = 1 : N$ **do**
18: $SOC_{i,end} \leftarrow SOC_0 - \sum_{j=1}^{i} \overline{k}_i^* s_i$
19: **end for**
20: **return** piecewise SoC reference trajectory on the spatial domain;

- The CDR on the energy domain is predicted based on Eqs. (23) and (24).
- Then $\overline{k}$ for each road section can be preliminarily predicted (lines $9 \sim 11$).
- The $\overline{k}$ needs to be fine-tuned to constrain it within the predicted boundary range, as illustrated in lines $12 \sim 16$.
- Finally, the discrete SoC points planned for each road sub-section are connected to form a piecewise linear trajectory, composing a global spatial-domain reference.

3.3.2. Comparison of explicit SoC planning algorithms

Based on different assumptions concerning charge depletion characteristics, SoC reference trajectory planning of global linear consumption on the spatial domain, global linear consumption and piecewise linear consumption on the energy domain, exhibit variable performance levels. Below, we compare the mechanisms of inspiration and applicable cycles for each SoC planning approach.

(1) Spatial-domain Linear SoC Planning Method (SL) [7,34,35]

Employing the concept of linear energy consumption in relation to distance traveled, this method formulates a linear State of Charge (SoC) reference trajectory that spans the entire route from origin to destination. Therefore, it necessitates only the acquisition of the remaining distance information obtained from ITS to plan the global trajectory of SoC. However, as noted in Section 2.2, the optimal CDR on the spatial domain is not a fixed value under specific driving cycles, indicating that the optimal SoC trajectory is also not linear on the spatial domain. Linear consumption characteristics of SoC trajectory on both the spatial and energy domains are only evident when the micro characteristics of the driving cycles exhibit uniformity on a global scale.

(2) Energy-domain Linear SoC Planning Method (EL) [26]

This method plans a trajectory from the origin to the destination that is linear on the energy domain but non-linear on the spatial domain, based on the global characteristic of linear depletion with driving energy. It requires predicted information from ITS with road section length, traffic flow speed, road gradient and etc. After segmenting the road sections, a piecewise linear global trajectory on the spatial domain is planned. This method assumes a constant CDR globally, which contradicts the analysis as above, and violate the law of CDR varies with power demanded. Therefore, this SoC planning method still losses optimality.

(3) Energy-domain Nonlinear SoC Planning Method (ENL) (Present Study)

Based on the micro-characteristics of nonlinear charge depletion with the average driving energy, this method, proposed in this study, plans a SoC reference trajectory that is nonlinear on both the spatial and energy domains over the whole journey. It requires predicted information from ITS about road section length, traffic flow speed, and global gradient, and after road segmenting, plans a piecewise linear SoC reference trajectory on the spatial domain. Compared to the above planning methods, this study more systematically analyzes the optimal charge depletion behaviors on both the energy and spatial domains and proposes an online SoC planning algorithm with solid theoretical backing. It should be noted that for road sub-sections governed by behavior '①', due to the lack of high-granularity power distribution prediction information, the precise range of charge depletion is challenging to predict, somewhat reducing the optimization potential. However, a reasonable prediction range can ensure that the SoC planning trajectory remains within a trackable area, with power split automatically

Table 3
Comparison of different SoC planning methods.

	SL	EL	ENL
Predictive Information	Mileage to destination	road sub-section mileage, traffic flow speed, elevation data	
Applicable cycles	Similar driving cycles over the journey	Pure electric or hybrid mode dominated driving cycles	All driving cycles

adjusted by the lower-level adaptive optimization to maintain high efficiency. A summarize of the required predictive information and applicable cycles for these three SoC planning methods is in Table 3.

4. Hierarchical framework for predictive energy management

4.1. Overview of the framework

To evaluate the performance of the aforementioned SoC planning methods, this study proposes a PEM strategy simulation framework, as depicted in Fig. 8.

4.2. Upper-level SoC planning

During the upper-level SoC planning stage, elevation data for the reference route is initially obtained using Google Earth software to calculate road grades; subsequently, the road network topology of the reference route is constructed using OpenStreetMap and imported into the SUMO (Simulation of Urban Mobility) [36] software for traffic scenario simulation. Real-time vehicle data, along with traffic and road length information and other data of V2X, are received in MATLAB through the TraCI4Matlab [36] communication interface. Using the predictive information provided by ITS, a global SoC reference trajectory is planned in MATLAB.

4.3. Lower-level power split

In the lower-level power-split stage, the PHEV's vehicle controller and powertrain are modeled in MATLAB/Simulink. Initially, a driver model controls the throttle and brake pedals to track the desired speed of the target vehicle in SUMO (Intelligent-Driver-Model [37] car-following model). Then, the ECU (Electronic Control Unit) sends drive power demand commands to the powertrain by interpreting pedal opening data. Finally, the power split module allocates drive energy demanded to the APU and battery according to these commands, with the output power from the APU and battery supplying the drive motor, which in turn drives the wheels, ultimately tracking the SoC reference trajectory while satisfying power demands. In the power split module, this study employs the Adaptive-PMP (A-PMP) for SoC tracking control. A-PMP regulates the value of the covariate λ through a discrete PI (Proportional Integral) controller with anti-integral windup:

$$\lambda(k) = \lambda_0 + \underbrace{k_p \times \left(SoC_{act}(k) - SoC_{ref}(k)\right)}_{proportion\ loop} + \underbrace{\lambda_i(k-1) + T \times k_i \times \left(SoC_{act}(k) - SoC_{ref}(k)\right) \times f(k)}_{integral\ loop} \tag{32}$$

where SoC_{act} and SoC_{ref} are the actual and reference SoC values respectively. The initial value of the covariate λ_0 is taken as -13500, the proportion gain k_p is taken as 100,000, and the integral gain k_i is taken as 200, λ_i denotes the control value of the integral loop, $f(k)$ is the anti-integral identifier, and T denotes the control step size. In this paper, clamping is used for the anti-integral windup, *i.e.*:

$$f(k) = \begin{cases} 0, & (P_{apu}(k-1) \geq P_{apu,max} \wedge SoC_{act}(k) > SoC_{ref}(k)) \\ & \vee (P_{apu}(k-1) \leq P_{apu,min} \wedge SoC_{act}(k) < SoC_{ref}(k)) \\ 1, & else \end{cases} \tag{33}$$

5. Simulations and discussions

In this section, the PEM framework is validated through Model-in-the-Loop (MiL) simulations. The simulations are performed on an experimentally-validated high-fidelity vehicle simulator [26], where shooting-based PMP algorithm [32] is applied to obtain the offline optimal solutions. Specifically, we use MATLAB to implement the control strategy of the power system, and SUMO [36] to construct the traffic environment in which the driving behavior is controlled by the IDM [37]. Some critical points are also discussed. We note that it is common practice to employ MiL simulation to verify and validate the design of control strategies before vehicle prototyping in the automotive industry [38,39].

5.1. Simulation setups

This study conducts simulation tests on three long-haul routes, incorporating a mix of urban, suburban, highway, and hilly driving cycles in Chongqing, Changsha, and Chengdu. Details of the routes, terrain, and vehicle speeds for these driving cycles are depicted in Fig. 9. Fig. 9.I presents the satellite images of the origins, destinations, and traffic light locations along the traveling routes. Fig. 9.II shows the elevation data segmented according to an ordered sample clustering algorithm, with segmentation points marked by gray asterisks "*". Among these, the road undulations of driving cycles in Chongqing experiences the most significant changes, followed by Chengdu, with Changsha having the most level terrain.

The OD-Matrix (Origin-Destination Matrix) describes the traffic volume at various entry and exit points along someone route, as shown in Table 4. For instance, the route in Chongqing includes 42 entries and exits, numbered 1 to 42. The first column lists the origin numbers, the first row lists the destination numbers, and the number "8" in the third row's last column indicates that eight vehicles per hour travel from origin 2 to destination 42.

The traffic flow velocity heatmap reflects changes in traffic conditions over time along the routes. As illustrated in Fig. 10, the target vehicle departs at various time under different driving cycles, traversing the predefined route's dynamic traffic environments and arriving at the destination. In this paper, the predetermined route is segmented according to the roadway speed limit and road grade, and the dynamic traffic flow speed is recorded at a regular interval (every 300 s) for each road section and the latest data is sent to EMS controller module of the target vehicle for SoC planning. It should be noted that the traffic conditions considered in this study are relatively fluid, and the impact of route curves on driving behavior is not considered since their influence on macroscopic speeds is minimal. The above road topology is provided by OpenStreetMap and edits the traffic scenario setups in SUMO.

5.2. Simulation results

5.2.1. Results for SoC planning

Due to the unpredictable dynamic changes in the traffic environment, it is not feasible to apply offline planning methods online. Therefore, this paper adopts the online SoC planning method outlined depicted in Section 3.3.1. The optimal one is only applicable to offline posterior planning after reaching the destination. This method plans the future SoC reference trajectories in a scrolling way based on real-time updated traffic flow speeds and fixed road gradients, with planning rolling triggered every 5 km of travel. As shown in Fig. 11, real-time planned and actual SoC trajectories for each driving cycles is represented by red dashed and blue solid lines, respectively. The first to the third rows are the trajectories at the first, sometime in the middle, and the last SoC planning instances. It is evident that the planned trajectories can be adjusted in real-time based on the dynamic changes

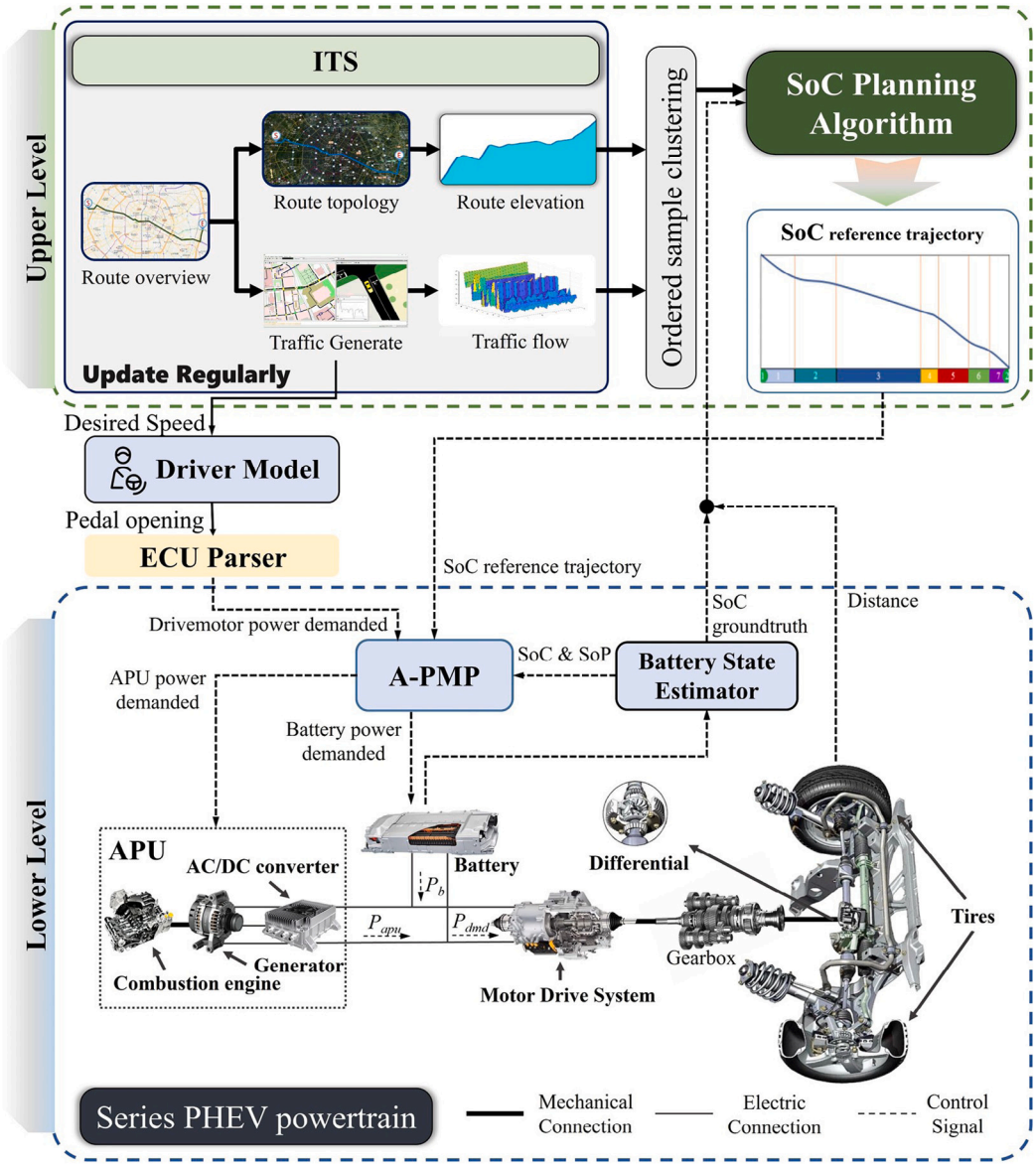

Fig. 8. Hierarchical predictive energy management strategy simulation framework.

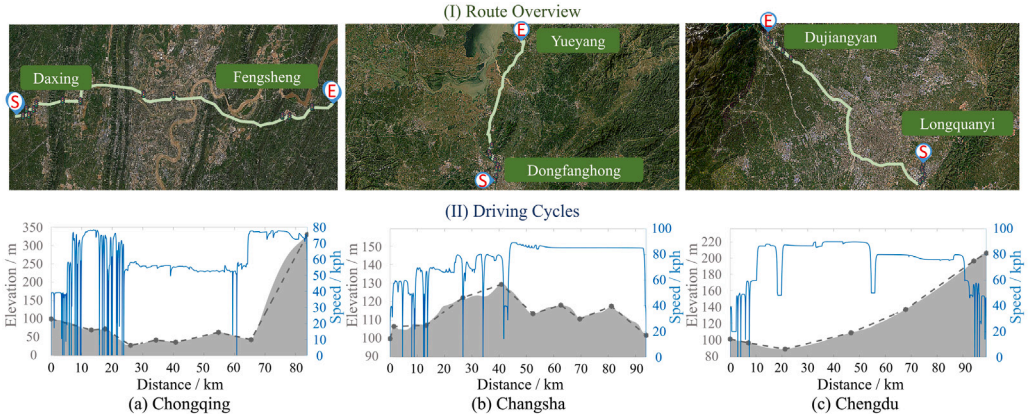

Fig. 9. Route overview and driving cycles of the three journeys.

Table 4
OD-Matrices.

(a) Chongqing

$O\backslash D$ $(vehs/h)$	1	2	...	42
1	\	6	...	10
2	\	\	...	8
...	...	...	...	...
42	\	\	...	\

(b) Changsha

$O\backslash D$ $(vehs/h)$	1	2	...	29
1	\	4	...	3
2	\	\	...	1
...	...	...	...	...
29	\	\	...	\

(c) Chengdu

$O\backslash D$ $(vehs/h)$	1	2	...	22
1	\	4	...	15
2	\	\	...	6
...	...	...	...	...
22	\	\	...	\

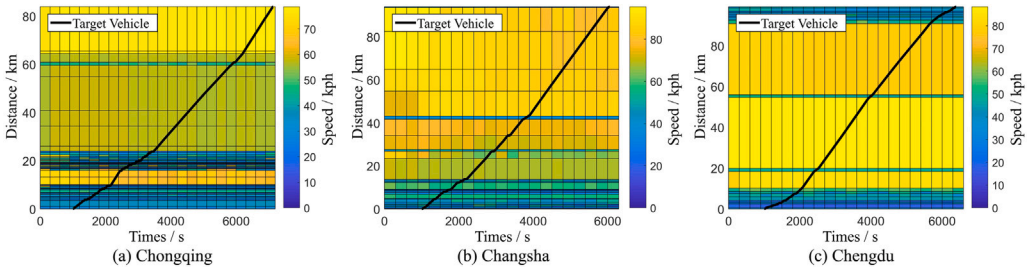

Fig. 10. Traffic flow velocity heatmap. (For interpretation of the references to color in this figure legend, the reader is referred to the web version of this article.)

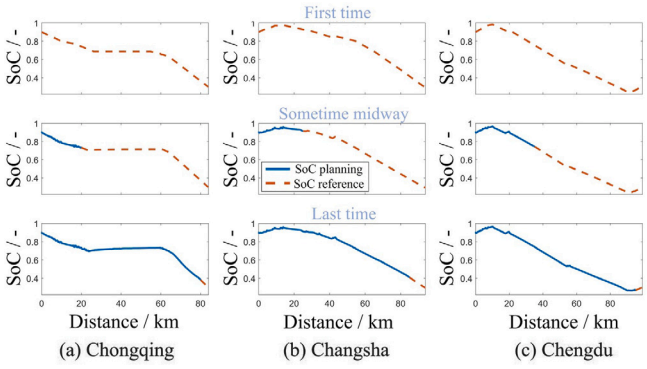

Fig. 11. Planning and reference trajectories of SoC.

in traffic flow, and actual trajectories tracks situation of historical reference well.

To compare the effectiveness of the SoC planning methods described in Section 3.3.2, the offline optimal PMP (OPT), SL, EL, act as the baselines to compare with the ENL algorithm proposed in this paper (all tracking methods employ A-PMP with unchanged parameters). As depicted in Fig. 12, the ENL proposed in this paper plans trajectories closely approximate the optimal trajectories. Simultaneously, the ENL method demonstrates superior SoC tracking effect thanks to the quasi-optimal reference for the lower-level power-split, outperforming the SL and EL methods much. It is due to the planning trajectories of SL and EL exceeding the operational capabilities of the powertrain, even with an overloaded workload the APU cannot supply sufficient power to the battery to track the reference SoC, such as beyond 70 km in Chongqing's driving cycles. Consequently, not only is the optimization effect of SL and EL methods poor, but they also fail to ensure the terminal SoC constraints.

5.2.2. Results for fuel consumption

Fuel economy is a core metric for evaluating EMS. The process fuel consumption in this study is obtained from the engine fuel consumption MAP lookup table. To fairly assess the global fuel economy, the difference between the actual terminal $SoC(end)$ and the desired value

Table 5
Fuel consumption.

Fuel Consumption/kg	OPT	SL	EL	ENL
Chongqing	15.002	15.384 (+2.544%)	15.212 (+1.400%)	15.064 (+0.407%)
Changsha	17.093	17.283 (+1.114%)	17.199 (+0.620%)	16.906 (−1.093%)
Chengdu	19.128	19.397 (+1.407%)	19.353 (+1.175%)	19.111 (−0.087%)

SoC_f is compensated for, estimating the terminal fuel consumption compensation as:

$$\Delta m_f = \frac{(SoC(end) - SoC_f)Q_{nom}\overline{V}_{oc}}{Q_{lhv}\overline{\eta}_{apu}} \tag{34}$$

where Δm_f is the fuel consumption correction; $\overline{V}_{oc}$ is the open-circuit voltage of the battery pack at an SoC of 0.6; the lower heating value of fuel Q_{lhv} is taken as 4.604×10^4 (J/g); $\overline{\eta}_{apu}$ is the average efficiency of the APU, set at 34.38%. Table 5 lists the fuel consumption for different SoC planning methods under various driving cycles, with the ENL method significantly reducing fuel consumption relative to SL and EL (the optimization effect exceeds 1.5% compared to SL), thus enhancing fuel economy. The reason why ENL shows lower fuel consumption than OPT in the Changsha and Chengdu driving cycles is due to some error in terminal fuel consumption compensation, but this does not affect the performance evaluation of the online planning algorithm. Since EL still retains some optimization capability, it achieves better fuel economy than SL, saving between 0.232% ∼ 1.144% in fuel, though its optimization effect is far less than that of ENL.

5.2.3. Results for real-time

Computation time is one of critical factors determining the feasibility of online applications. Fig. 13 records the planning time for each driving cycles at different travel distances, with single calculation time generally on the order of 10^{-3} s and gradually decreasing as the planning distance reduces. Relative to the offline optimal PMP computation time (Chongqing: 897 ± 167 s; Changsha: 529 ± 140 s; Chengdu: 661 ± 174 s), the ENL method introduced in this study delivers substantial fuel savings and requires minimal computational effort. This positions the ENL method as highly suitable for real-time onboard applications.

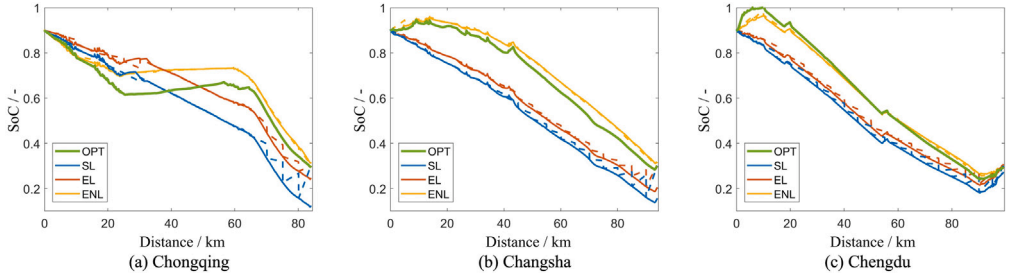

Fig. 12. SoC trajectories. Solid lines represent actual SoC trajectories, and dashed lines represent planned SoC trajectories. The colors for actual and planned trajectories of the same planning algorithm are consistent (OPT — optimal trajectory, SL — spatial domain linear planning, EL — energy domain linear planning, ENL — energy nonlinear domain planning). (For interpretation of the references to color in this figure legend, the reader is referred to the web version of this article.)

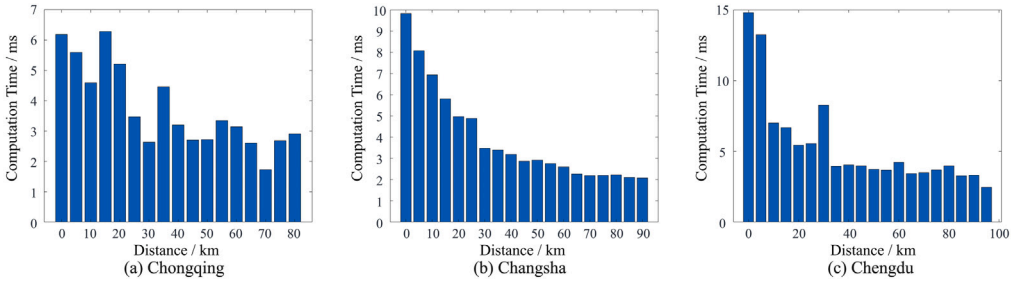

Fig. 13. The computation time for each planning along the routes.

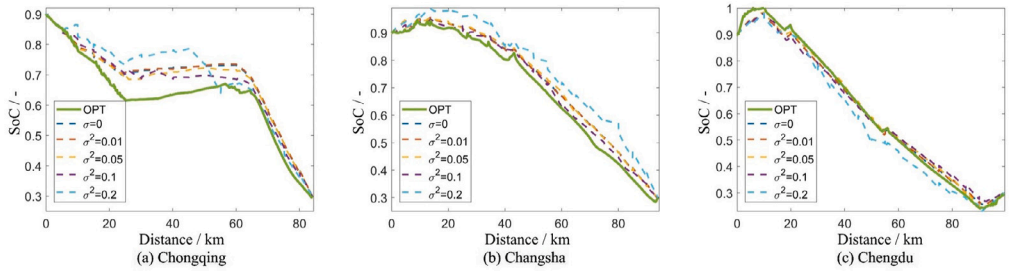

Fig. 14. Comparison of the planned and optimal SoC trajectories under different Gaussian noise superimposed on traffic flow prediction speeds. (For interpretation of the references to color in this figure legend, the reader is referred to the web version of this article.)

5.3. Discussions and susceptibility

Robustness of SoC planning algorithms is one of the critical metrics for evaluating the performance. This study introduces the ENL method, which is influenced by traffic flow speed prediction information and the segmentation of road gradients using an ordered sample clustering algorithm. An analysis of the sensitivity of the algorithm to perturbations in various parameters is as follows:

1. Traffic flow speed

In Section 5.1, based on standard traffic flow speeds, different levels of Gaussian noise ($N(\mu, \sigma^2), \mu = 0, \sigma^2 = 0.01, 0.05, 0.1, 0.2$) were added to analyze the sensitivity of the planning effectiveness to perturbations in traffic flow speed prediction information, and the comparison of its global planning and optimal trajectory as shown in Fig. 14. The SoC planning trajectories gradually deviate from the optimum as the noise increases. However, this change is not significant when $\sigma^2 \leq 0.1$. Fuel consumption results are illustrated in Fig. 15, the trends upward or fluctuate slightly with increasing noise, yet it still retains a significant economic advantage over the SL and EL methods. Hence, the ENL method proposed in this paper demonstrates strong resilience against traffic flow speed prediction errors.

2. Road segmentation

The length of road gradient segmentation determines the granularity of terrain prediction information, which directly affects SoC planning optimization. By manually segmenting roads with different granularity (segmentation interval: 0.5 km, 1 km, 10 km, 20 km), and study their impact on SoC planning trajectories (as shown in Fig. 16) and fuel consumption (as shown in Fig. 17). The impact of granularity of road section segmentation on SoC planning trajectories is minimal. In driving cycles such as Changsha and Chengdu, virtually nothing has changed, while the slight visible change in Chongqing's planning trajectories is mainly due to its relatively significant road undulations, making the planning trajectories more susceptible to the granularity of road gradient prediction information. However, the variations in fuel consumption are minimal, with a slight upward trend as the granularity of road gradients decreases, but this increase is very minimal. Therefore, the ENL method proposed in this paper is not significantly affected by the granularity of road gradient segmentation. The use of an ordered sample clustering algorithm allows for clustering of adjacent road sections with similar terrains, reducing the number of road sections and improving computational efficiency.

In summary, the ENL planning method proposed is not sensitive to the aforementioned two factors and exhibits good robustness.

6. Conclusions

In addressing the problem of charge planning within predictive energy management, this study pioneers an explicit piecewise linear

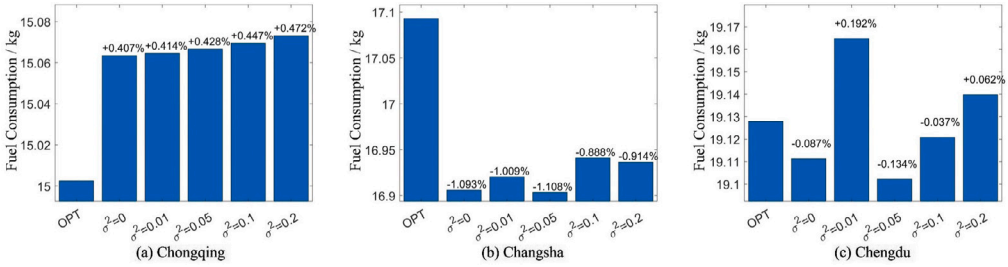

Fig. 15. Fuel consumption results.

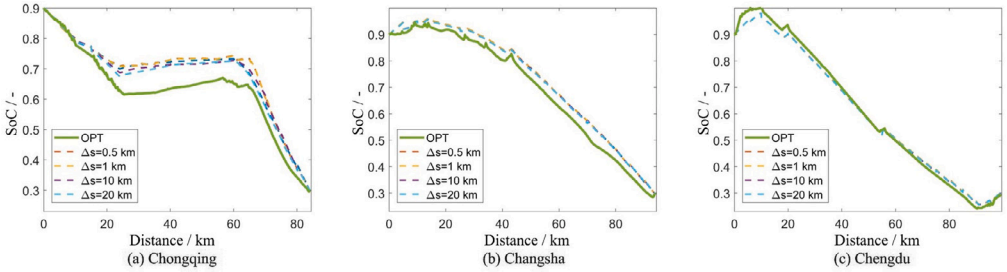

Fig. 16. Comparison of the planned and optimal SoC trajectories under different granularity of road segmentation. (For interpretation of the references to color in this figure legend, the reader is referred to the web version of this article.)

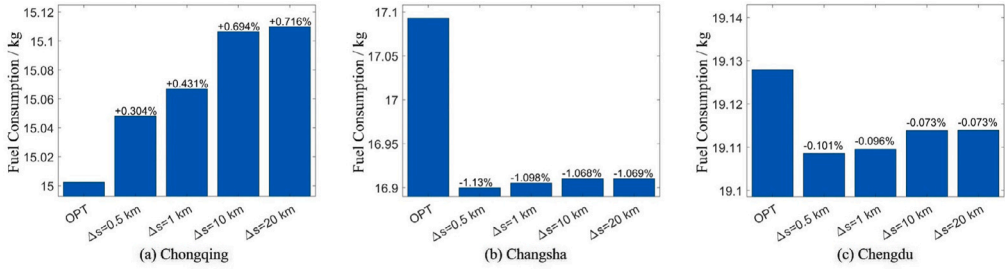

Fig. 17. Fuel consumption results under different road granularity.

SoC reference trajectory planning solution on the spatial domain. It is achieved through leveraging predicted methodologies and terminal conditions essential for ascertaining optimal charge depletion rates on the energy domain, culminating in the formulation of an explicit equation for optimal decline rates of SoC on the spatial domain. By synthesizing the mechanism of optimal charge depletion behavior on the spatial domain with experienced boundary constraints — aimed at minimizing optimality loss — a piecewise linear SoC reference trajectory planning approach was engineered to mitigate dependence on high-granularity predictive data for road segments with fluctuating driving power demand levels. This algorithm was seamlessly integrated into a comprehensive closed-loop PEM framework and subjected to rigorous numerical validation on a high-fidelity MiL platform. Compared with offline optimal and alternative online planning baselines, the method proposed exhibits superior performance by closely approximating global optimal SoC trajectories and yielding a minimum of 1.5% in fuel consumption savings against traditional linear strategies. It also stands out for its reduced computational load and augmented robustness.

Nonetheless, the SoC planning approach delineated in this study is not devoid of limitations. Primarily, its application is confined to series hybrid powertrain, with extrapolation to disparate configurations necessitating additional research endeavors. Furthermore, it is imperative for the PEM strategy to undergo verification through hardware-in-the-loop experimental evaluations. In the future, our endeavors will be channeled towards surmounting these challenges to foster the development of high-performance PEM solutions, drawing upon the insights elucidated in this study.

CRediT authorship contribution statement

Xuan Cai: Writing – original draft, Visualization, Software, Resources, Methodology. **Wei Zhou:** Funding acquisition, Conceptualization, Methodology. **Zhiyong Cui:** Writing – review & editing, Supervision, Methodology. **Xuesong Bai:** Writing – review & editing, Supervision, Resources. **Fan Liu:** Writing – review & editing, Visualization, Software. **Haiyang Yu:** Supervision, Investigation, Funding acquisition. **Yilong Ren:** Supervision, Resources, Investigation.

Declaration of competing interest

The authors confirm that there are no conflicts of interest arising from consultancy, patents, products in development, or marketed products related to the content of this document. No relationships or activities exist that could undermine the objectivity or integrity of the research findings and conclusions.

Acknowledgments

The authors would like to appreciate the financial support of the Natural Science Foundation of Hunan Province (2022JJ30158) and the National Key Research and Development Project of China under Grant 2022YFB4300400.

Data availability

Data will be made available on request.

References

[1] Yoshizawa Takahito, Singelée Dave, Muehlberg Jan Tobias, Delbruel Stephane, Taherkordi Amir, Hughes Danny, et al. A survey of security and privacy issues in v2x communication systems. ACM Comput Surv 2023;55(9):1–36.

[2] Han Jie, Shu Hong, Tang Xiaolin, Lin Xianke, Liu Changpeng, Hu Xiaosong. Predictive energy management for plug-in hybrid electric vehicles considering electric motor thermal dynamics. Energy Convers Manage 2022;251:115022.

[3] Ju Fei, Murgovski Nikolce, Zhuang Weichao, Hu Xiaosong, Song Ziyou, Wang Liangmo. Predictive energy management with engine switching control for hybrid electric vehicle via admm. Energy 2023;263:125971.

[4] Han Jie, Liu Wenxue, Zheng Yusheng, Khalatbarisoltani Arash, Yang Yalian, Hu Xiaosong. Health-conscious predictive energy management strategy with hybrid speed predictor for plug-in hybrid electric vehicles: Investigating the impact of battery electro-thermal-aging models. Appl Energy 2023;352:121986.

[5] Cordiner Stefano, Galeotti Matteo, Mulone Vincenzo, Nobile Matteo, Rocco Vittorio. Trip-based soc management for a plugin hybrid electric vehicle. Appl Energy 2016;164:891–905.

[6] Guo Ningyuan, Zhang Xudong, Zou Yuan, Guo Lingxiong, Du Guodong. Real-time predictive energy management of plug-in hybrid electric vehicles for coordination of fuel economy and battery degradation. Energy 2021;214:119070.

[7] Tang Xiaolin, Jia Tong, Hu Xiaosong, Huang Yanjun, Deng Zhongwei, Pu Huayan. Naturalistic data-driven predictive energy management for plug-in hybrid electric vehicles. IEEE Trans Transp Electrification 2020;7(2):497–508.

[8] Jinquan Guo, Hongwen He, Jiankun Peng, Nana Zhou. A novel mpc-based adaptive energy management strategy in plug-in hybrid electric vehicles. Energy 2019;175:378–92.

[9] Piras M, Bellis V De, Malfi E, Desantes Jose M, Novella M. Incorporating speed forecasting and soc planning into predictive ecms for heavy-duty fuel cell vehicles. Int J Hydrog Energy 2024;55:1405–21.

[10] Han Wenxiao, Chu Xiaohua, Shi Sui, Zhao Ling, Zhao Zhen. Practical application-oriented energy management for a plug-in hybrid electric bus using a dynamic soc design zone plan method. Processes 2022;10(6):1080.

[11] Onori Simona, Tribioli Laura. Adaptive pontryagin's minimum principle supervisory controller design for the plug-in hybrid gm chevrolet volt. Appl Energy 2015;147:224–34.

[12] Ma Yangyang, Wang Pengyu, Sun Tianjun. Research on energy management method of plug-in hybrid electric vehicle based on travel characteristic prediction. Energies 2021;14(19):6134.

[13] Yang Chao, Du Siyu, Li Liang, You Sixong, Yang Yiyong, Zhao Yue. Adaptive real-time optimal energy management strategy based on equivalent factors optimization for plug-in hybrid electric vehicle. Appl Energy 2017;203:883–96.

[14] Zhang Hao, Lei Nuo, Liu Shang, Fan Qinhao, Wang Zhi. Data-driven predictive energy consumption minimization strategy for connected plug-in hybrid electric vehicles. Energy 2023;283:128514.

[15] Wang Yue, Li Keqiang, Zeng Xiaohua, Gao Bolin, Hong Jichao. Investigation of novel intelligent energy management strategies for connected heb considering global planning of fixed-route information. Energy 2023;263:125744.

[16] Guo Ningyuan, Shen Jiangwei, Xiao Renxin, Yan Wensheng, Chen Zheng. Energy management for plug-in hybrid electric vehicles considering optimal engine on/off control and fast state-of-charge trajectory planning. Energy 2018;163:457–74.

[17] Zhao Nan, Zhang Fengqi, Yang Yalian, Coskun Serdar, Lin Xianke, Hu Xiaosong. Dynamic traffic prediction-based energy management of connected plug-in hybrid electric vehicles with long short-term-state of charge planning. IEEE Trans Veh Technol 2023.

[18] Lin Yang, Chu Liang, Hu Jincheng, Zhang Yuanjian, Hou Zhuoran. An intelligent energy management strategy for plug-in hybrid electric vehicle inspired from monte carlo tree search. In: 2022 IEEE 25th international conference on intelligent transportation systems. IEEE; 2022, p. 811–6.

[19] Wang Rong, Shi Xianrang, Su Yang, Song Tinglun. A predictive energy management strategy for plug-in hybrid electric vehicles using real-time traffic based reference soc planning. Proc Inst Mech Eng D 2024;09544070241239996.

[20] Montazeri-Gh Morteza, Pourbafarani Zeinab. Near-optimal soc trajectory for traffic-based adaptive PHEV control strategy. IEEE Trans Veh Technol 2017;66(11):9753–60.

[21] Hu Donghai, Cheng Shan, Zhou Jiaming, Hu Leli. Energy management optimization method of plug-in hybrid-electric bus based on incremental learning. IEEE J Emerg Sel Top Power Electron 2021;11(1):7–18.

[22] He Hongwen, Huang Ruchen, Meng Xiangfei, Zhao Xuyang, Wang Yong, Li Menglin. A novel hierarchical predictive energy management strategy for plug-in hybrid electric bus combined with deep deterministic policy gradient. J Energy Storage 2022;52:104787.

[23] Min Qingyun, Li Junqiu, Liu Bo, Li Jianwei, Sun Fengchun, Sun Chao. Guided model predictive control for connected vehicles with hybrid energy systems. Energy 2021;230:120780.

[24] Kuchly Jean, Simon Antoine, Jaine Thierry, Nelson-Gruel Dominique, Charlet Alain, Nouillant Cédric, et al. Analytical solution and soc reference planning for energy and pollutants management of plug-in hybrid electric vehicles. In: 2020 IEEE conference on control technology and applications. IEEE; 2020, p. 423–9.

[25] Nunzio Giovanni De, Sciarretta Antonio, Gharbia Ibtihel Ben, Ojeda Luis Leon. A constrained eco-routing strategy for hybrid electric vehicles based on semi-analytical energy management. In: 2018 21st international conference on intelligent transportation systems. IEEE; 2018, p. 355–61.

[26] Zhou Wei, Chen Yaoqi, Zhai Haoran, Zhang Weigang. Predictive energy management for a plug-in hybrid electric vehicle using driving profile segmentation and energy-based analytical soc planning. Energy 2021;220:119700.

[27] Zhou Wei, Cai Xuan, Chen Yaoqi, Li Junqiu, Peng Xiaoyan. Decoding the optimal charge depletion behavior in energy domain for predictive energy management of series plug-in hybrid electric vehicle. Appl Energy 2022;316:119098.

[28] Mahmoodi-k Mehdi, Montazeri Morteza, Madanipour Vahid. Simultaneous multi-objective optimization of a phev power management system and component sizing in real world traffic condition. Energy 2021;233:121111.

[29] Zhou Wei, Zhang Chengning, Li Junqiu, Fathy Hosam K. A pseudospectral strategy for optimal power management in series hybrid electric powertrains. IEEE Trans Veh Technol 2015;65(6):4813–25.

[30] Zhou Wei, Zhang Ningfeng, Zhai Haoran. Enhanced battery power constraint handling in mpc-based hev energy management: A two-phase dual-model approach. IEEE Trans Transp Electrification 2021;7(3):1236–48.

[31] Lv Chen, Zhang Junzhi, Li Yutong, Yuan Ye. Mechanism analysis and evaluation methodology of regenerative braking contribution to energy efficiency improvement of electrified vehicles. Energy Convers Manage 2015;92:469–82.

[32] Zhang Fengqi, Hu Xiaosong, Langari Reza, Cao Dongpu. Energy management strategies of connected hevs and PHEVs: Recent progress and outlook. Prog Energy Combust Sci 2019;73:235–56.

[33] Fisher Walter D. On grouping for maximum homogeneity. J Am Stat Assoc 1958;53(284):789–98.

[34] Xie Shaobo, Hu Xiaosong, Xin Zongke, Li Liang. Time-efficient stochastic model predictive energy management for a plug-in hybrid electric bus with an adaptive reference state-of-charge advisory. IEEE Trans Veh Technol 2018;67(7):5671–82.

[35] Zhou Shiyao, Chen Ziqiang, Huang Deyang, Lin Tiantian. Model prediction and rule based energy management strategy for a plug-in hybrid electric vehicle with hybrid energy storage system. IEEE Trans Power Electron 2020;36(5):5926–40.

[36] Lopez Pablo Alvarez, Behrisch Michael, Bieker-Walz Laura, Erdmann Jakob, Flötteröd Yun-Pang, Hilbrich Robert, Lücken Leonhard, Rummel Johannes, Wagner Peter, Wießner Evamarie. Microscopic traffic simulation using sumo. In: The 21st IEEE international conference on intelligent transportation systems. IEEE; 2018, URL https://elib.dlr.de/124092/.

[37] Kesting Arne, Treiber Martin, Helbing Dirk. Enhanced intelligent driver model to access the impact of driving strategies on traffic capacity. Phil Trans R Soc A 2010;368(1928):4585–605.

[38] Ekhtiari Sanaz, Faieghi Mohammadreza, Azad Nasser Lashgarian. Sensitivity analysis of a real-time trip planning assisted energy management system for connected plug-in hybrid electric vehicles. IEEE Trans Veh Technol 2019;68(8):7340–52.

[39] Wang Hanchen, Arjmandzadeh Ziba, Ye Yiming, Zhang Jiangfeng, Xu Bin. Flexnet: A warm start method for deep reinforcement learning in hybrid electric vehicle energy management applications. Energy 2024;288:129773.